ORIGINAL ARTICLE

Open Access

Exploring changes in building strength using seismic wave deconvolution

Yu-Ting Chou[1], Strong Wen[2,3]* , Chun-Fu Liao[2], Ying Nien Chen[2] and Chun-Hsiang Kuo[4,5,6]

Abstract

In order to avoid the casualties caused by damaged buildings during strong earthquakes, it's important and essential to understand the seismic design specifications of buildings. The motion of a building depends on the interferometry of building and ground motion, the coupling between building and ground, and the mechanical properties of the building. We applied deconvolution technique to the motion recorded to separate the building response and calculated the structural parameters (including traveling wave velocity, resonant frequency and attenuation parameter). Therefore, we can check medium's state by tracking these parameters to avoid damaged building collapse in the next mega-earthquake. We deployed a seismograph array in the building to record the earthquakes and few months of ambient noise data. In addition, we divided the structure into lower and higher floors to calculate the layering velocity. We found that the wave velocities of the lower and higher floors are significantly different but the former exhibit stable variation. For the monitoring phase, we tried different stacking time-lengths and calculated the related traveling wave velocities which are similar to the analysis in earthquakes. From the above results, we concluded that the physical parameters of the building can monitor the healthy condition of structure. Finally, we hope these results would be helpful to build a long-term monitoring of building's healthy status and the assessment of seismic hazard.

Keywords Building response, Traveling wave velocity, Resonant frequency, Attenuation, Ambient noise

1 Introduction

Recently, because of the high-density seismograph network, we have learned more about the active fault structure in Taiwan, but we have also noticed the high potential of the earthquake disasters. Due to the high economic development in Taiwan, the population density and the number of high-rise buildings is increasing year by year, which may lead to more serious disaster risks. The 2016 Meinong earthquake in Taiwan caused buildings to collapse and killed hundreds of people; the 2018 Hualien earthquake and 2022 Guanshan-Chishang earthquake caused severe damage to the buildings around the fault trace (see Fig. 1). Therefore, in order to avoid damage to buildings caused by severe earthquakes and casualties, it is essential to monitor the earthquake resistance of buildings.

Snieder and Şafak (2006) extracted building response from seismic record to calculate building's traveling wave velocity and attenuation parameter (Q-value) by applying deconvolution to seismic record. Nakata et al. (2015) estimated building's fundamental mode from the building response. Traveling wave velocity reflects the shear strength of the medium (Todorovska and

*Correspondence:
Strong Wen
strong@eq.ccu.edu.tw; strong6212@gmail.com
[1] Graduate School of Engineering, Kyoto University, Kyoto, Japan
[2] Department of Earth and Environmental Sciences, National Chung Cheng University, No. 168, Sec. 1, University Rd., Min-Hsiung Township, Chiayi 621, Taiwan, ROC
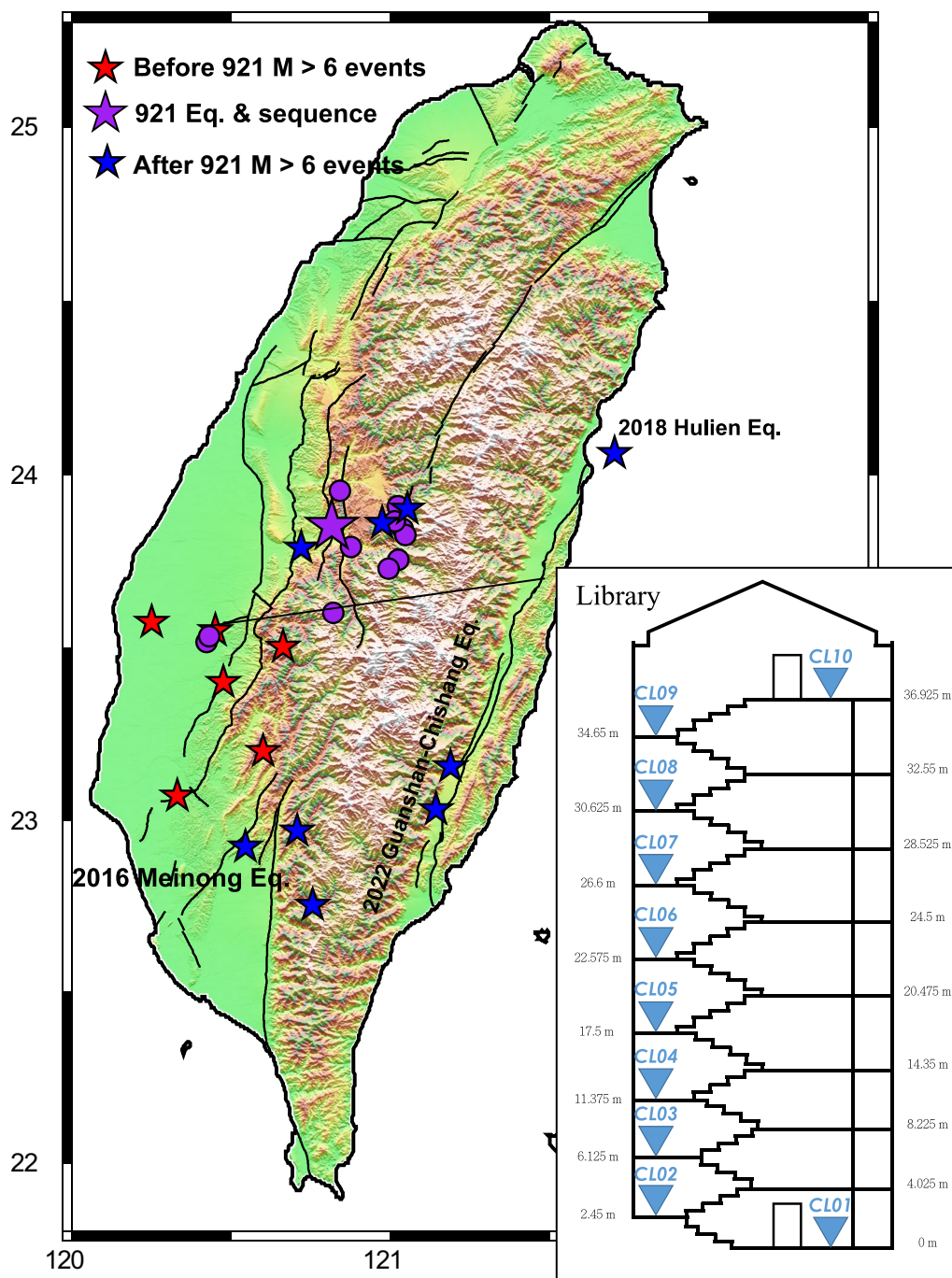[3] Southern Taiwan Earthquake Center, National Chung Cheng University, Chiayi, Taiwan
[4] Department of Earth Sciences, National Central University, Taoyuan, Taiwan
[5] Earthquake-Disaster and Risk Evaluation and Management Center, National Central University, Taoyuan, Taiwan
[6] National Center for Research On Earthquake Engineering, Taipei, Taiwan

Fig. 1 Distribution map of historical earthquakes (M > 6) in the area where the library is located and the adjacent areas. The map shows that numerous catastrophic earthquakes have occurred in the area surrounding the subject building in the past and recent years. Therefore, monitoring buildings is indeed an urgent task. The lower right illustration shows the distribution of the monitoring stations within the library building

Trifunac 2008a), fundamental mode is often used to detect changes in the state of building (Maeck and Roeck 1999) and the Q-value reflects the degree of the attenuation of the energy inside the building, which is affected by

the cracks and pore water inside the medium (Feng et al. 2015). These parameters (traveling wave velocity, resonant frequency and Q-value) allow us to build a structural health monitoring (SHM) system by tracking them

before and after earthquakes and investigate whether the buildings are damaged (Mucciarelli et al. 2004; Todorovska and Trifunac 2008a, b; Picozzi et al. 2011; Nakata et al. 2015; Rahmani et al. 2015; Kohler et al. 2018; Sun et al. 2019). On the other hand, Prieto et al. (2010) and Nakata and Snieder (2014) applied deconvolution technique to ambient noise record and estimated the traveling wave velocity, resonant frequency and Q-value. This approach enables us to break through the limit of uncertainty of seismic sources and provide stable sources to establish a continuous monitoring system (Mordret et al. 2017; Lacanna et al. 2019).

In this study, we used the library on the campus of National Chung Cheng University (CCU) of Taiwan as an experimental site and deployed an array of seismometers. The library is located nearby an active fault called Meishan Fault which caused the 1906 Meishan earthquake (M_L 7.1) and led to serious earthquake disaster (see Figs. 1 and 2). In Fig. 1, the map shows that numerous catastrophic earthquakes (M > 6) have occurred in the area surrounding the subject building in the past and recent years. Therefore, monitoring buildings is indeed an urgent task. We applied deconvolution technique to the seismic record, calculated and monitored the
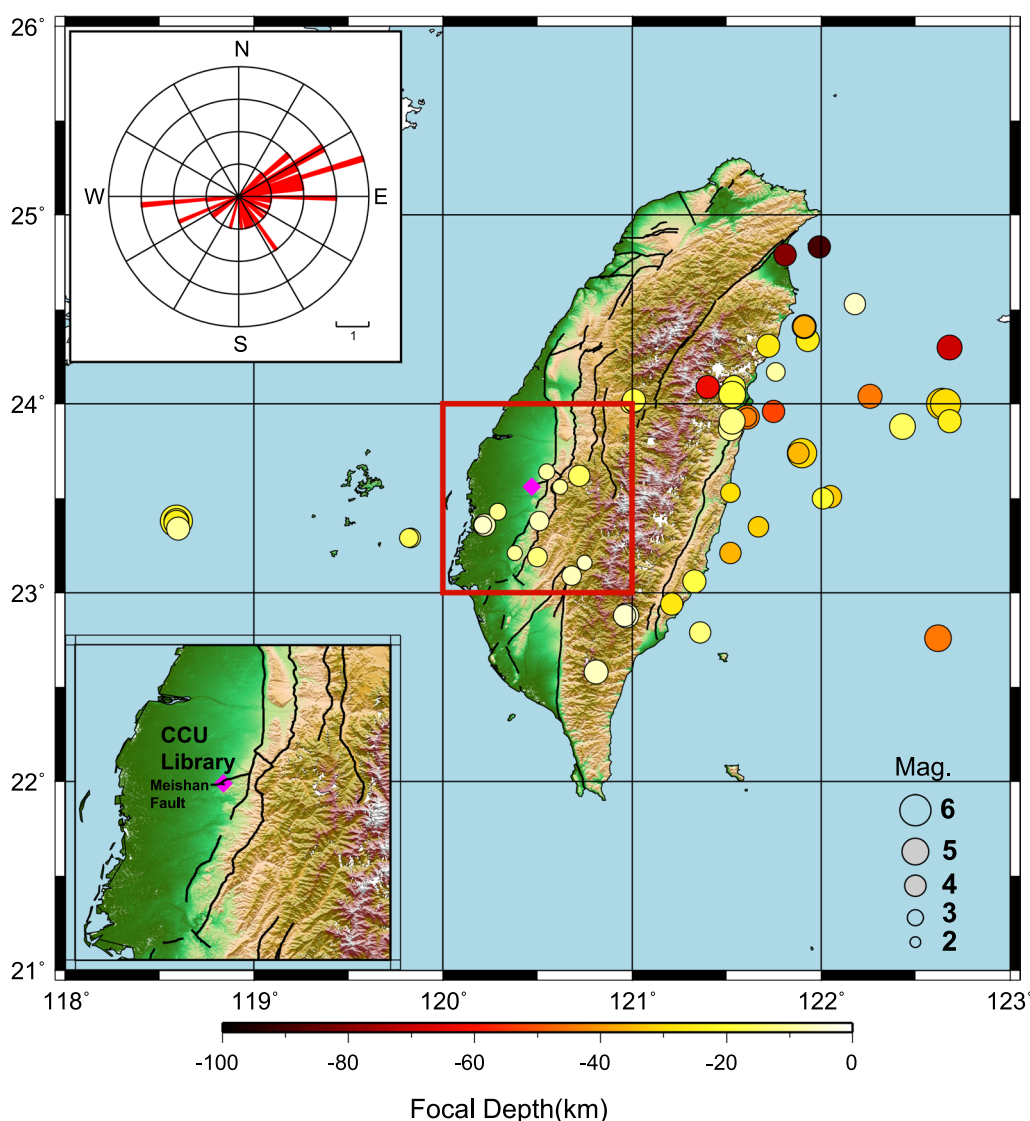
Fig. 2 The total number of seismic events used in this study is approximately to 56. The epicenter of each event is represented by a circle, where the color and diameter represent the focal depth and magnitude, respectively. The pink square indicates the location of the library which is near by the Meishan Fault, and the black lines indicate the active fault in Taiwan. The rose diagram shows the back-azimuthal distribution of seismic events. Its length change in radius indicates the number of earthquakes in a certain direction

structural parameters (traveling wave velocity, resonant frequency and Q-value) during observation period. We also promoted the temporal resolution of the monitoring system and made it approximated to near real-time monitoring which allow us to detect damage immediately. In previous studies, we considered changes in the structural parameters of the building and the degree of damage, and set a threshold for the monitoring system to identify whether the building was damaged.

2 Data and method

The library is an eight-story reinforced concrete building built in 1989 (see Fig. 1, right panel), which is located nearby an active fault called Meishan fault so its seismic resistance was enhanced and could withstand a maximum 0.4 g of peak ground acceleration. Therefore, this study was instrumented with 10 boardband seismographs (Meridian Compact PostHole) with sampling rate 100 Hz, recording earthquakes and ambient noise records from 2018/09 to 2019/01. These seismographs were placed on the the library in the direction of the vertical line. Due to the limitation of the structure of staircase, station CL01 and CL10 were placed at the position about 3 m away from the vertical line (Fig. 1).

We compared the earthquake records received by our array and the earthquake catalog of the Central Weather Administration, chose up the earthquake events with larger magnitude and closer epicenter distance from the library (Fig. 2). We then integrated the records to displacement domain and passed 0.1–10 Hz

Butterworth bandpass filter. Figure 3 shows the time–frequency energy diagram of the vibration record at CL10 station, in which areas with stronger energy are concentrated at several specific frequency locations of the library. Therefore, we let the continuous ambient noise records passed 1–7 Hz Butterworth bandpass filter to keep the main tones and filtered the noise in high frequencies to improve the precision of picking.

In the study we took these parameters as our criteria to discuss and monitor health condition of the library. In Snieder and Şafak (2006) study, applying deconvolution to earthquake record could be written as:

$$\mathrm{D}(\omega) = \frac{u_1(\omega)u_2^*(\omega)}{|u_2(\omega)|^2 + \varepsilon}$$

where $u_1(\omega)$, $u_2(\omega)$ are two arbitrary signals in frequency domain, * indicates the complex conjugation and ε is a constant which set to 10% of the average spectral power. Here, they can be regarded as seismic wave signals from different responses. We then applied picking and FFT (Fast Fourier Transform) to the extracted building response and calculated the traveling wave velocity and its spectrum (Fig. 4). From Snieder and Şafak's (2006) equation, we know that the waveform deconvolved by basement's record could be written as:

$$B(z,t) \approx \frac{4\pi c}{\mathrm{H}} \exp(-\gamma\omega_0 t) \cos\left(\frac{\omega_0(H-z)}{c}\right) \sin(\omega_0 t)$$

with
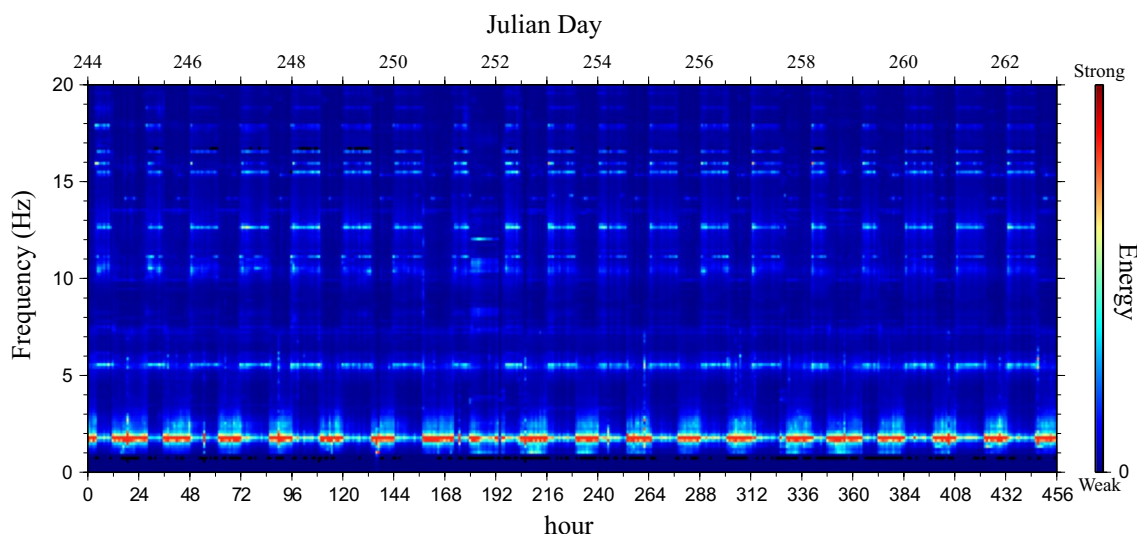
Fig. 3 The spectrogram of station CL10. The time interval of data was Julian day 244 to 262 and the time resolution was 1 h. Background's color from warm to cool which indicated the energy level from high to low. The energy patterns reflected the open and close time of the library, seismic events and the tones of the library
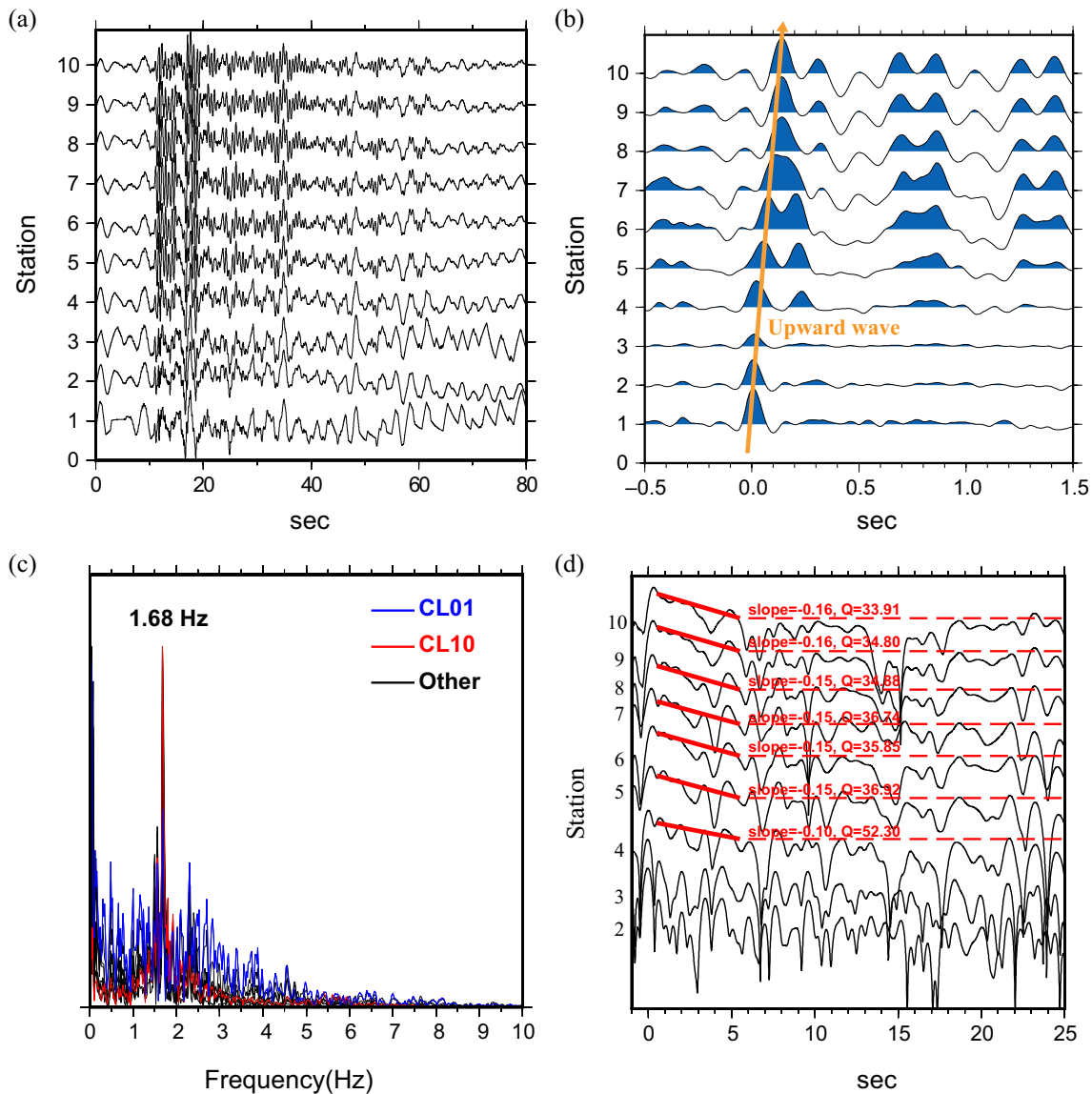
Fig. 4 An earthquake event occurred in 2019/01/11, its epicenter located at 120.62°E, 23.56°N where the epicenter distance was 16.5 km and the magnitude was 2.9 in M_L. **a** The earthquake's NS component waveform in displacement which been applied 0.1–10 Hz Butterworth bandpass filter. **b** The deconvolved waveform of (**a**). We pick up the deconvolved waveform and calculate its apparent velocity and the arrow indicates the direction. **c** The spectrum of the earthquake. The blue, red and black lines represent the spectrum of station CL01, CL10 and others stations, respectively. **d** The schematic diagram of the attenuation parameter (Q-value). The waveform in this figure is the natural logarithm of the envelope of the waveform in **b**. The solid red line represents the slope of the wave attenuated to noise level at each station (red dashed line). We ignored the lower stations to avoid incomplete decoupling situations

$$\omega_0 = \frac{\pi c}{2H}$$

where $B(z, t)$ is the deconvolved waveform of station at height z, c is the traveling wave velocity, ω_0 is the fundamental mode, H is the height of the building and γ is the damping ratio. Where the slope of the deconvolved waveform is related to Q-value:

$$\gamma = \frac{1}{2Q}$$

Therefore, we could calculate the Q-value through the deconvolved waveform. After applying the 1–3 Hz Butterworth filter to the deconvolved waveform, the slope can be estimated by the natural logarithm of its envelope through the least square's method. The equation between the slope and Q-value is:

$$Slope = \frac{-\omega_0}{2Q}$$

here we average the Q-values of the stations to obtain the attenuation factor of the building for each earthquake. We excluded the Q-values of station (CL01, CL02, and CL03) on lower floors to avoid incomplete decoupled between the library and the ground. We found that the deconvolved waveform of the EW component shown reversed wave phases from station CL06 (Fig. 5), we believed this might due to the library's structure (there is atrium garden locate between station CL05 and CL06). Therefore, in this study we concentrated on the data of NS component to avoid the opposite wave phases interfere with others.

For the ambient noise issue, Nakata and Snieder (2014) applied deconvolution to ambient noise:

$$D_{noise}(z,t) \approx \sum_{n=1}^{N} \left[F^{-1} \left\{ \frac{u_n(z,\omega)u_n^*(0,\omega)}{|u_n(0,\omega)|^2 + \alpha \langle|u_n(0,\omega)|\rangle^2} \right\} \right]$$

where N is the total number of time windows, F^{-1} indicated inverse Fourier transform, $\langle|u_n|\rangle^2$ is the average power spectrum of u_n and $\alpha = 0.5\%$. In this study we deconvolved with the record of the station on roof:

$$D_{noise}(z,t) \approx \sum_{n=1}^{N} \left[F^{-1} \left\{ \frac{u_n(z,\omega)u_n^*(H,\omega)}{|u_n(H,\omega)|^2 + \varepsilon} \right\} \right]$$

where time window is 30 s. We stacked the deconvolved noise signal to improve S/N ratio where we quoted the similarity equation of Prieto et al. (2010) and Nakata and Snieder (2014):

$$\text{Misfit}(z,h) = \sqrt{\frac{\int_{t_a}^{t_b}[D_h(z,t) - D_{all}(z,t)]^2 dt}{\int_{t_a}^{t_b}[D_{all}(z,t)]^2 dt}}$$

where h is the stacked time interval, t_a and t_b are set to be -1.5 s and 1.5 s, D_{all} is the reference waveform which is the deconvolved and stacked result of entire data. In Fig. 6, the results showed the diagram of misfit and stacked duration. We referred to Nakata and Snieder (2014) study and took the data that stacked over 96 h as a reliable result and applied picking to calculate traveling wave velocity.

Therefore, the method to calculate velocity is to first pick the arrival time according to the maximum amplitude of the deconvolved waveform for each floor, then calculate the traveling velocity according to the arrival time and the height of each floor. For seismic events, only considered the arrival time for one way up (CL01 to CL10). For ambient noise, due to the stacked deconvolved waveform has clear peaks, we considered the round-trip data (CL01 to CL10 to CL01) to obtain a more stable and convergent result.
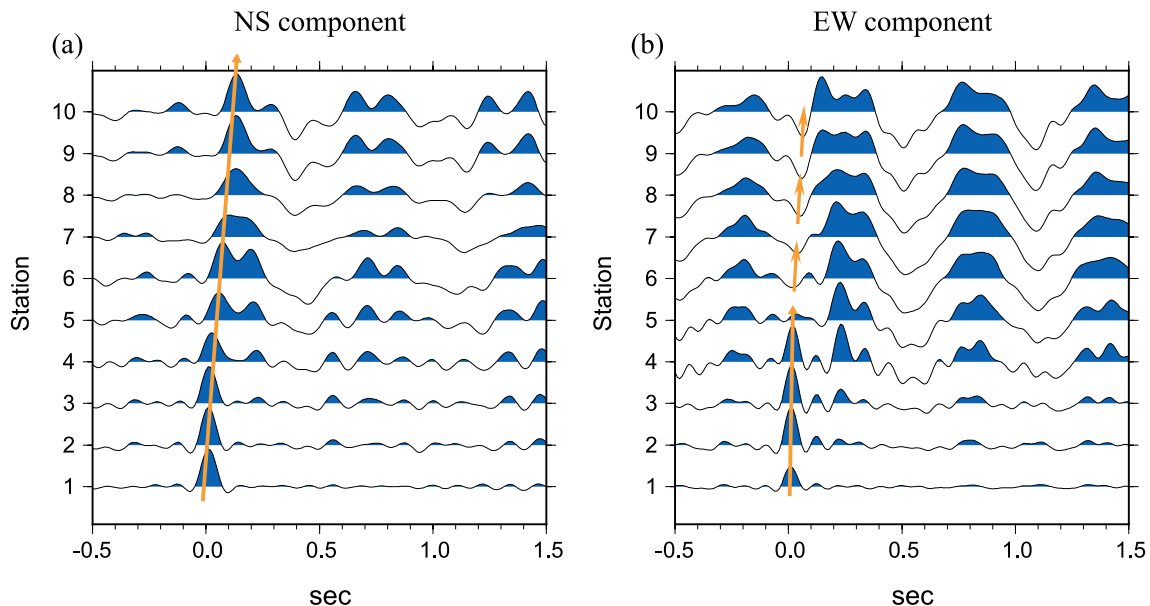
Fig. 5 The deconvolved waveform of (**a**) NS component and (**b**) EW component. Arrowhead indicated their wave directions and the dash arrowhead indicated the wave which changed phase around station CL05 and CL06. We believe this is caused by the internal structure of the library
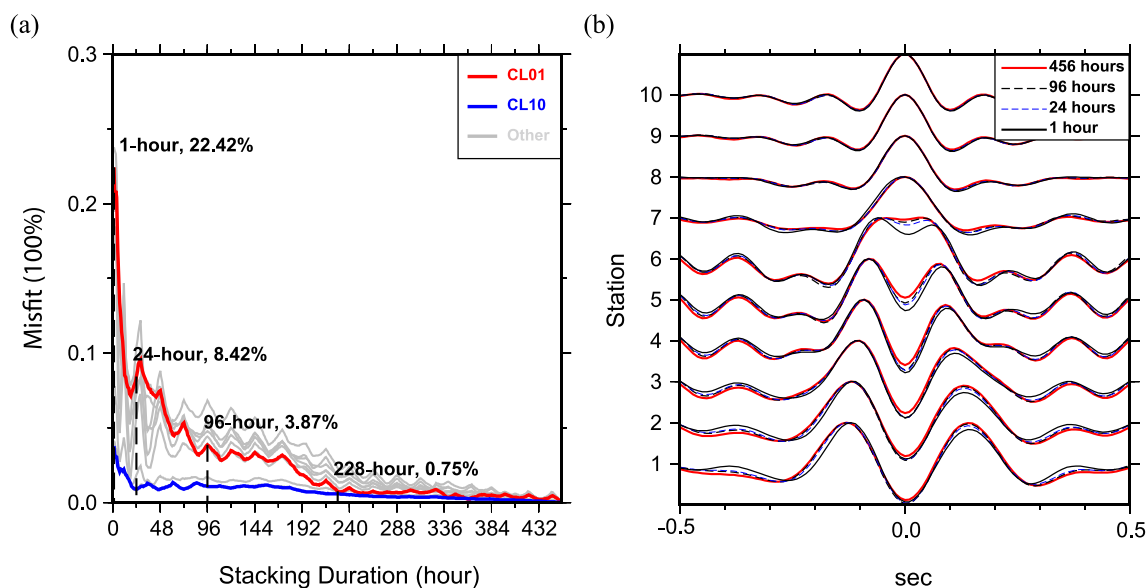
Fig. 6 a The relationship between misfit (100%) and stacking duration (hour). The reference waveform is the deconvolved waveform stacked from Julian day 244 to 262 (456 h totally) which was the longest continuous observation in this study. Red, blue and gray line indicated the misfit of station CL01, CL10 and the other stations, respectively. The dash lines indicated the misfit of each stacking duration. **b** The waveforms for different stacking durations. The red solid line indicated the deconvolved waveform stacked for 456 h, black dash line indicated the deconvolved waveform stacked for 96 h, and so on. These waveforms were similar to each other which indicated similar wave velocity. The asymmetry in amplitude between causal and acausal waveform might due to the uneven distribution of noise sources

3 Result

In this study, we applied deconvolution technique to earthquake records, separate the building response and used it to calculate the structural parameters (including traveling wave velocity, resonant frequency and Q-value). The results were integrated in Fig. 7. These parameters were consistent under stable condition but may be changed when the building is damaged (Khoo et al. 2004; Todorovska and Trifunac 2008a, b; Feng et al. 2015). The wave velocity related to the physical parameters of medium, such as bulk modulus, shear modulus and Young's modulus. The resonant frequency related to building's structure, mass, strength and the coupling with ground. It may also be changed when the coupling between building and ground has been changed (Clinton 2004). The attenuation parameter (or Q-value) reflects the attenuation of wave energy, it is affected by the states of cracks and pore water in the medium. If earthquakes increase the density of crack inside the building or the state of pore water has been changed, it will be response on the Q-value; the closer to fracture, the greater the variation of Q-value (Feng et al. 2015). Therefore, we could take these parameters as the indicators of building's state. On the other hand, we also applied deconvolution technique to ambient noise record and calculated wave velocities (Table 1). The velocities shown stable and convergent variation which indicated the library was in stable condition. We had tried different

stacking durations and found that although the stacking durations were less than the similarity equation suggested, the stacking results shown identically (Fig. 6) which led to similar velocities. The slightly different of waveform of station CL06 may due to the change of different sources (for instance, different source pattern in library's open and close hours, tide and weather changing). Therefore, we tested different stacking durations and estimated their wave velocities. From the data of testing results, it was considered that 1 h of stacking duration may be enough to calculate wave velocity ($v_{1-hour} = 284.22 \pm 13.75 m/s$, $v_{96-hour} = 292.18 \pm 6.70 m/s$). The range of standard deviation is also smaller than the changes of wave velocities caused by the damage of buildings in previous studies. The portion of library's traveling wave velocities each hour and under earthquake event were shown in Fig. 8. We found the velocities often shown discontinuous change before and after library's open and close hours (gray and white boundary). We believed it was related to the changing of sources pattern and the energy amplitude of ambient noise (such as air conditioner switching, human activities, etc.). We could also see the traveling wave velocity decreased during seismic events and returned to previous value after the earthquakes which indicated that the library has not been damaged by the earthquakes. But due to the lack of strong earthquake data during the observation period, it is impossible to analyze the changes in the main resonance
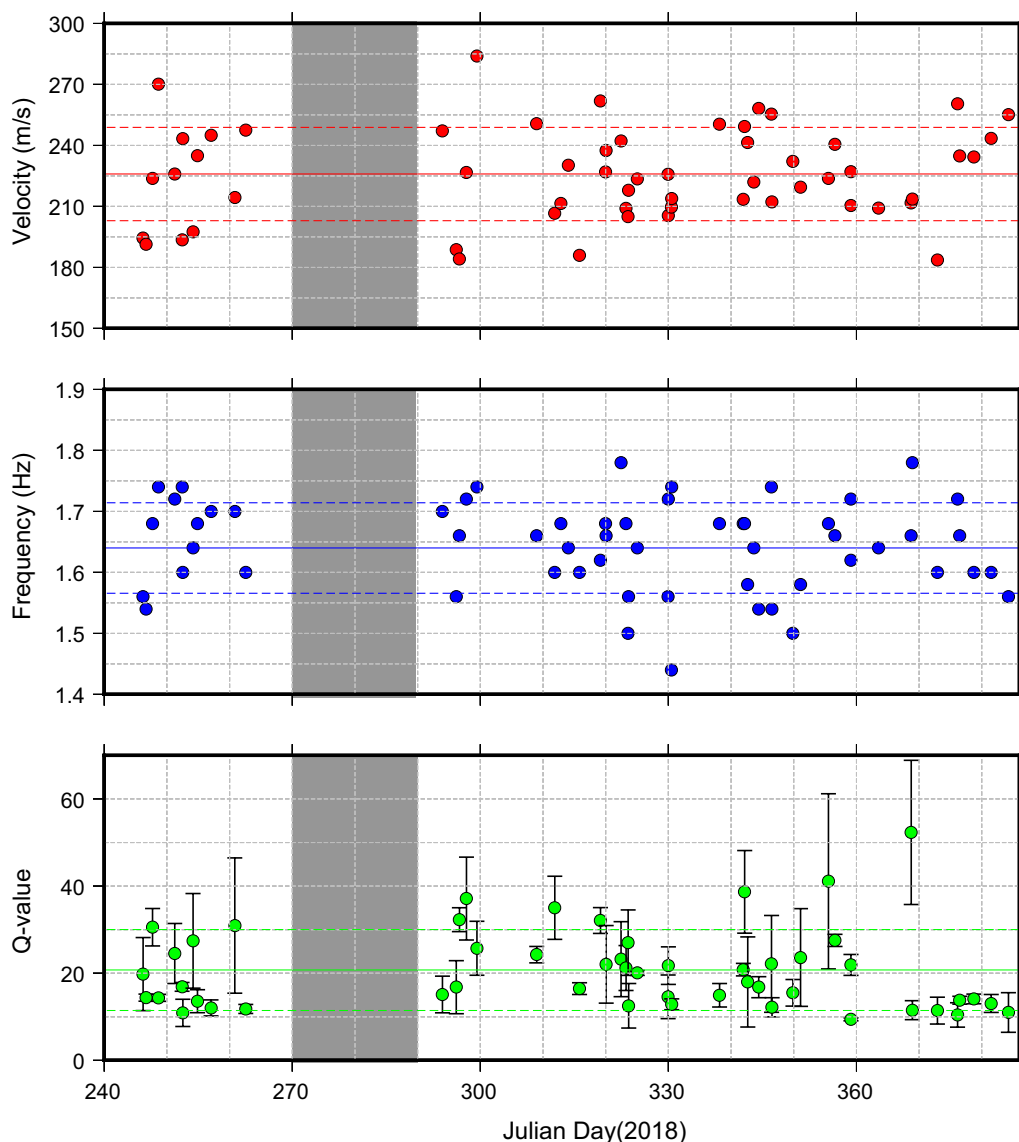
Fig. 7 Structural parameters (including traveling wave velocity, fundamental frequency and attenuation parameter) calculated from earthquake records. Each circle represents the results of each seismic event. The error bar of Q-value represents the standard deviation of the Q-values for the floors. Solid and dashed lines are the average and standard deviation of all seismic events. There is a data gap between Julian day 270 and 290 due to the exhaustion of the battery (the gray zone)

frequency of the building. In addition, we also calculated the layering velocity with ambient noise data stacked 24 h, hoping to locate potential damage locations (Fig. 9). Therefore, this study can improve the possibility of daily monitoring of buildings through the analysis of weak motions.

4 Discussion

In this study, we calculated the structural parameters of a reinforced concrete building with earthquake and ambient noise records. From Figs. 5 and 9, seismic waves propagating up and down in a building can reflect the

effects caused by their path, and waves reflected from the horizontal direction can be ignored (Todorovska and Trifunac 2008a). It can be seen that the wave phase changes between the measuring stations CL05 and CL06. Since the physical properties of the library are RC building, the structure also has an atrium above the 5th floor, the waves exhibit different propagation speeds on high floors and low floors. In addition to the atrium structure above the 5th floor, the material differences caused by the large area of glass curtains are also responsible for the differences in wave propagation speed. From the results,

**Table 1** Velocities of deconvolved waveform stacked 96 h

Julian day	Velocity (m/s)
2018/244~247	301.60
2018/248~251	300.78
2018/252~255	303.14
2018/256~259	296.16
2018/259~262	298.82
2018/285~288	284.03
2018/289~292	290.01
2018/292~295	295.80
2018/297~300	293.39
2018/305~308	293.06
2018/309~312	276.48
2018/314~317	292.46
2018/318~321	291.39
2018/322~325	280.43
2018/326~329	283.44
2018/333~336	282.66
2018/337~340	284.18
2018/341~343	293.17
2018/346~349	291.37
2018/350~353	292.58
2018/355~358	295.01
2018/362~365	288.98
2019/001~004	295.82
2019/005~007	298.66
2019/009~012	297.95
2019/013~016	295.82
2019/017~020	291.73
Average	292.18±6.70

we could build a structural health monitoring system through calculating and tracking these parameters to avoid damaged building collapse during earthquakes. Seismic records provided the building responses under actual earthquakes, while ambient noise provided continuous sources which allowed us to build a near real-time monitoring system. In this study we also integrated the structural parameters of observed and experiment cases from previous studies (Fig. 10, Table 2). The types of the buildings inside the listed previous studies are reinforced concrete buildings except one is a slice of RC building (Ebrahimian et al. 2017). However, we believe that the method utilized in this study could be widely applied to different types of buildings. Because this method only requires the deployment of seismometers inside a building, and it does not require the assumption of building type. This is an advantage for structural health monitoring because researchers won't have to spend large amount of time and money to customize their monitoring system for each different case.

We also drawn the distribution of the changing degree of structural parameters before and after building damaged and their damage grades in EMS-98 scale (Grünthal and Levret 2001) according to the descriptions in previous studies (Fig. 11, Tables 3 and 4). Some of the damage descriptions in previous studies were not detailed so we considered its stiffness changing degree and related damage grades (Maeck and Roeck 1999; Okada and Takai 2000; Rossetto and Elnashai 2003). In Fig. 11, it could be seen that the structural parameters' changing degrees increased with damage grades consistently both in shake table experiments and actual observed cases. We considered the building with damage grade 3 or higher requires
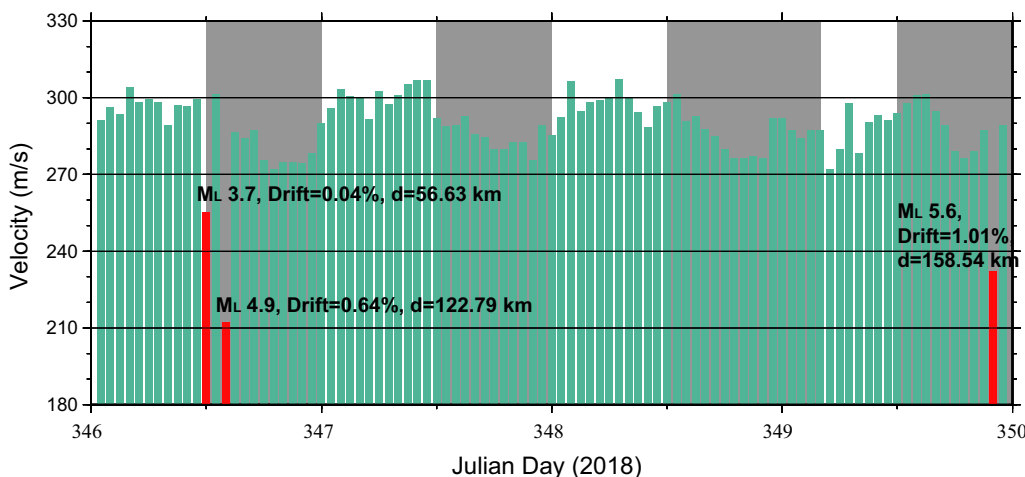
Fig. 8 Traveling wave velocity of each hour calculated from ambient noise (green bar) and earthquake events (red bar). Each red bar was marked with its related event's magnitude, library's drift and epicentral distance. Background's white and gray area indicated the library's open and close hours
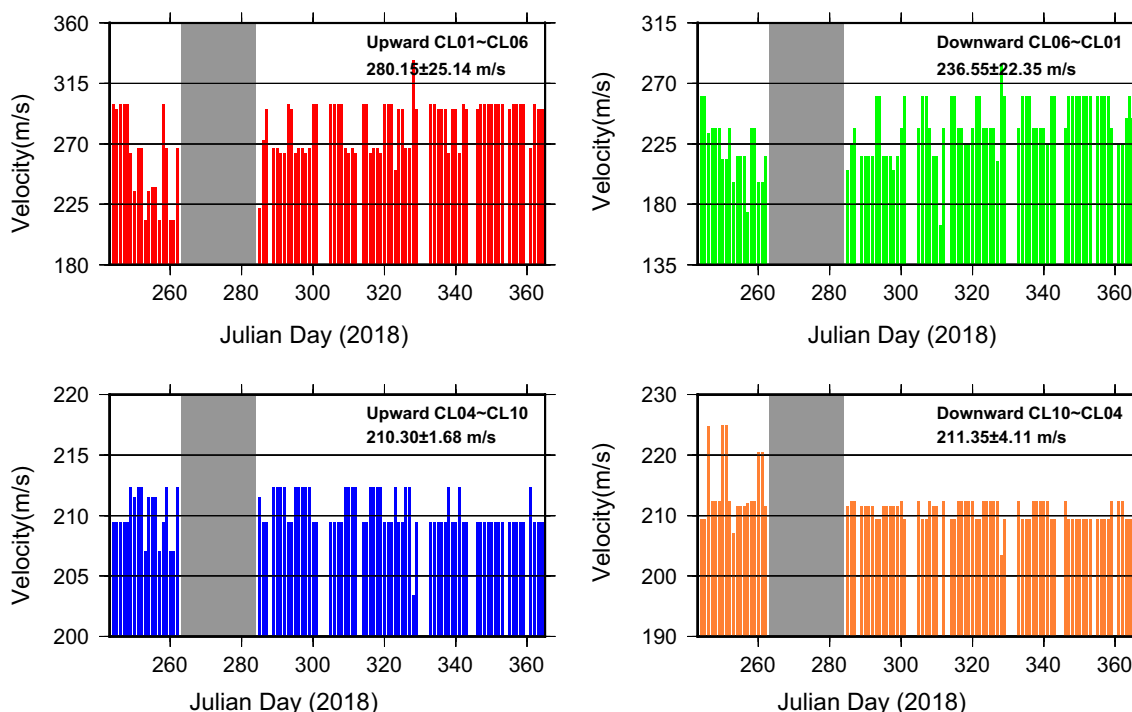
Fig. 9 The layering velocity of the library every 24 h. The gray zone was lacked of data. There were gaps between the velocities of upward and downward waves which might due to different boundary condition of upper and lower part of the library, even so the velocities still maintained a stable distribution

vigilance. Therefore, we regard the velocity changed degree reach 30% or resonant frequency changed degree reach 20% as a warning line. The wave velocity and resonant frequency of the library were stable during our observation, even if an earthquake occurred and the library was drifted more than 1.25% (Naeim and Kelly 1999). Therefore, we believe it indicates that the library was in stable condition and there was no damage due to the earthquakes.

Among the structural parameters, the Q-value shows relatively high uncertainty in average (see Fig. 7c). Also, the standard deviation of Q-value for some earthquakes also high. Although those events with higher averaged Q-values seems to have higher uncertainty, we do not find any clear relation or trend between Q-value and other parameters (e.g., peak velocity on top floor, building drift, and back azimuth of seismic events). Besides, we shortened the stacking duration of ambient noise to build a near real time monitoring system so one could detect damage occur immediately; furthermore, we calculated the layering velocity to locate the potential damage. The accuracy of layering velocity is depended on the sampling rate of the instrument, distance between sensors, frequency range selecting and sensors' density. In general, higher sampling rate and denser sensors can yield more accurate results; nevertheless, one should also consider the budget limit for the monitoring system. Building array could use to monitor the health condition of the building and provide precious data like waveform record, pick ground acceleration, pick ground velocity, building drift, shaking time, power spectrum density, etc. These data may help the monitoring system to improve its criteria for detecting damage and further study and also provide valuable information for future study.

5 Conclusion

In this study, we used a seismograph array in a library to record five months of earthquake and ambient noise data. We applied deconvolution technique to the records and separated the building responses for calculating the structural parameters, including traveling wave velocity, resonant frequency and attenuation parameter. Structural parameters are affected by the structure itself and physical parameter of the building such as shear strength, bulk modulus and Young's modulus. By tracking these parameters, we could monitor the health condition of the building. Earthquake record provided the building response under actual earthquake event and ambient noise record provided us continuous sources to build the near real time monitoring system. From above results, the library's structural parameters shown stable and convergent variation. However, the range of the variation of

(a)

(b)
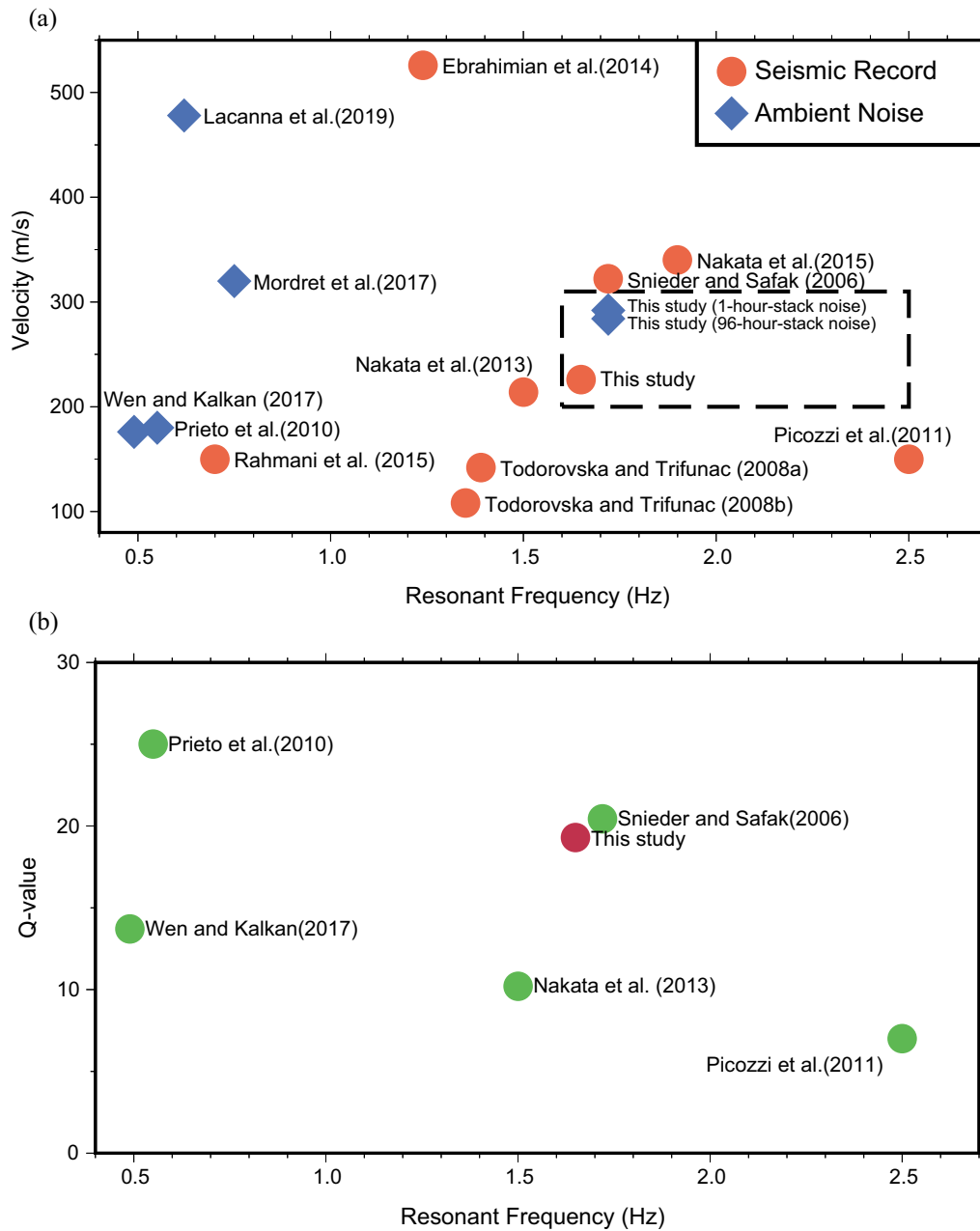
Fig. 10 a The distribution diagram of velocities and resonant frequencies of previous studies and the results of this study. Circle indicated the parameter was calculated from earthquake record and diamond indicated it was calculated from ambient noise. **b** The distribution diagram of Q-values and resonant frequencies of previous studies and results of this study

the calculated results is much smaller than the structural parameters in the case of earthquake damage in previous studies. Therefore, our results were similar to previous studies which indicated the application of the method on different types of buildings. On the other hand, we raised the S/N ratio by stacking the ambient noise result and we found that although the stacking duration was far less than the convergent test suggested, we could still earn reliable results. The shorter stacking duration allowed us to build a near real time monitoring system which could detect the damage occurred immediately and allow us to make a prompt response.
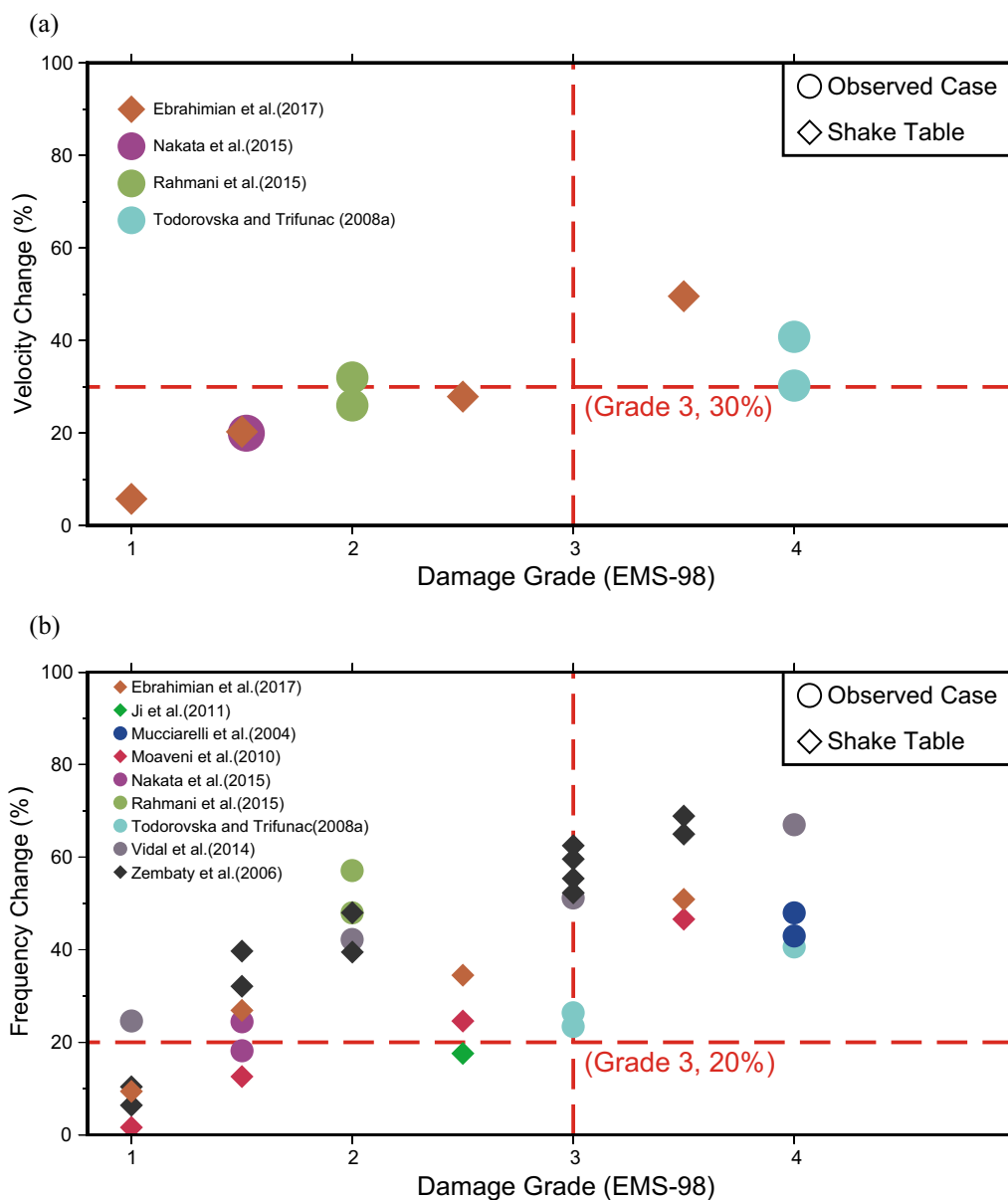
Fig. 11 The diagram of (**a**) velocity and (**b**) resonant frequency changing degree related to the damage grade in EMS-98 scale. Circle indicated the data was from actual observation and diamond indicate the data was from shake table test. In the previous research, we classified the damage level according to the description of the damage or the change in stiffness, and for the ambiguous situation, we placed it between the two levels

Table 2 Structural parameters in previous studies and this study, the lack of result was marked with none

Source	Height (m)	Velocity (m/s)	Resonant frequency (Hz)	Q-value	Data type
Snieder and Safak (2006)	43.9	322	1.72	20.45	Earthquake
Todorovska and Trifunac (2008a)	25.5	142	1.39	(None)	Earthquake
Todorovska and Trifunac (2008b)	20	108.2	1.35	(None)	Earthquake
Prieto et al. (2010)	71	180	0.55	25	Ambient noise
Picozzi et al. (2011)	7	150	2.5	7	Earthquake
Nakata et al. (2013)	38.95	214	1.5	25	Earthquake
Ebrahimian et al. (2014)	39	526	1.24	(None)	Earthquake
Rahmani et al. (2015)	48.5	150	0.7	(None)	Earthquake
Nakata et al. (2015)	47	340	1.9	(None)	Earthquake
Ebrahimian et al. (2017)	19.2	1030	1.92	(None)	Ambient noise
Mordret et al. (2017)	83.7	320	0.75	(None)	Ambient noise
Wen and Kalkan (2017)	80.54	176	0.49	15.1	Ambient noise
Lacanna et al. (2019)	84	478	0.62	(None)	Ambient noise
This study	36.925	226	1.65	19.30	Earthquake
This study	36.925	284	1.72	(None)	Ambient noise
This study	36.925	292	1.72	(None)	Ambient noise

Data type indicated these parameters were calculated from earthquake or ambient noise record

Table 3 The changing degree of velocity of damaged building in previous study

Source	Initial value (m/s)	Damaged value (m/s)	Changing degree	Damage grade
Todorovska and Trifunac (2008a)	142	84	40.8%	Grade 4
Todorovska and Trifunac (2008a)	208	145	30.3%	Grade 4
Rahmani et al. (2015)	110	74.8	32%	Grade 2
Rahmani et al. (2015)	140	103.6	26%	Grade 2
Nakata et al. (2015)	(None)	(None)	~20%	Grade 1 or 2
Ebrahimian et al. (2017)	1030	970	5.8%	Grade 1
Ebrahimian et al. (2017)	1030	821	20.3%	Grade 1 or 2
Ebrahimian et al. (2017)	1030	743	27.9%	Grade 2 or 3
Ebrahimian et al. (2017)	1030	519	49.6%	Grade 3 or 4

The damaged grade was in EMS-98 scale

Table 4 The changing degree of frequency of damaged building in previous study

Source	Initial value (Hz)	Damaged value (Hz)	Changing degree	Damage grade
Todorovska and Trifunac (2008a)	2.27	1.67	26.4%	Grade 3
Todorovska and Trifunac (2008a)	1.92	1.47	23.4%	Grade 3
Todorovska and Trifunac (2008a)	1.92	1.14	40.6%	Grade 4
Vidal et al. (2014)	(None)	(None)	24.6%	Grade 1
Vidal et al. (2014)	(None)	(None)	42.2%	Grade 2
Vidal et al. (2014)	(None)	(None)	51.2%	Grade 3
Vidal et al. (2014)	(None)	(None)	67%	Grade 4
Rahmani et al. (2015)	(None)	(None)	48%	Grade 2
Rahmani et al. (2015)	0.7	0.3	57.1%	Grade 2
Nakata et al. (2015)	2.2	1.8	18.2%	Grade 1 or 2
Nakata et al. (2015)	2.38	1.8	24.4%	Grade 1 or 2
Mucciarelli et al. (2004)	2.5	1.3	48%	Grade 4
Mucciarelli et al. (2004)	3.2	1.8	43%	Grade 4
Moaveni et al. (2010)	1.91	1.88	1.6%	Grade 1
Moaveni et al. (2010)	1.91	1.67	12.6%	Grade 1 or 2
Moaveni et al. (2010)	1.91	1.44	24.6%	Grade 2 or 3
Moaveni et al. (2010)	1.91	1.02	46.6%	Grade 3 or 4
Ji et al. (2011)	0.51	0.42	17.6%	Grade 2 or 3
Ebrahimian et al. (2017)	1.71	1.55	9.4%	Grade 1
Ebrahimian et al. (2017)	1.71	1.25	26.9%	Grade 1 or 2
Ebrahimian et al. (2017)	1.71	1.12	34.5%	Grade 1 or 3
Ebrahimian et al. (2017)	1.71	0.84	50.9%	Grade 3 or 4

The damaged grade was in EMS-98 scale

Declarations

Competing interests
The authors acknowledge there are no conflicts of interest recorded.

References

Clinton JF (2004) Modern digital seismology: instrumentation, and small amplitude studies in the engineering world. EERL Report, 2004–10, Earthquake Engineering Research Laboratory, Pasadena, CA

Ebrahimian M, Rahmani M, Todorovska MI (2014) Nonparametric estimation of wave dispersion in high-rise buildings by seismic interferometry. Earthquake Eng Struct Dynam 43:2361–2375

Ebrahimian M, Todorovska MI, Falborski T (2017) Wave method for Struct Health Monit: testing using full-scale shake table experiment data. J Struct Eng 143:04016217

Feng Q, Kong Q, Huo L, Song G (2015) Crack detection and leakage monitoring on reinforced concrete pipe. Smart Mater Struct 24:115020

Grünthal G, Levret A (2001) L'Echelle Macrosismique Européenne. European Macroseismic Scale 1998 (EMS-98). Cahiers du Centre Européen de Géodynamique et de Séismologie 19, Centre Européen de Géodynamique et de Séismologie, Luxembourg, 103

Ji X, Fenves GL, Kajiwara K, Nakashima M (2011) Seismic damage detection of a full-scale shaking table test structure. J Struct Eng 137:14–21

Khoo LM, Mantena PR, Jadhav P (2004) Structural damage assessment using vibration modal analysis. Struct Health Monit 3:177–194

Kohler M, Allam A, Massari A, Lin FC (2018) Detection of building damage using Helmholtz tomography. Bull Seism Soc Am 108(5A):2565–2579

Lacanna G, Ripepe M, Coli M, Genco R, Marchetti E (2019) Full structural dynamic response from ambient vibration of Giotto's bell tower in Firenze (Italy), using modal analysis and seismic interferometry. NDT and E Int 102:9–15

Maeck J, De Roeck G (1999) Dynamic bending and torsion stiffness derivation from modal curvatures and torsion rates. J Sound Vib 225:153–170

Moaveni B, He X, Conte JP, Restrepo JI (2010) Damage identification study of a seven-story full-scale building slice tested on the UCSD-NEES shake table. Struct Saf 32:347–356

Mordret A, Sun H, German A, Prieto A, Nafi Toksöz M, Büyüköztürk O (2017) Continuous monitoring of high-rise buildings using seismic interferometry. Bull Seism Soc Am 107:2759–2773

Mucciarelli M, Masi A, Gallipoli MR, Harabaglia P, Vona M, Ponzo F, Dolce M (2004) Analysis of RC building dynamic response and soil-building

resonance based on data recorded during a damaging earthquake (Molise, Italy, 2002). Bull Seism Soc Am 94:1943–1953

Nakata N, Snieder R (2014) Monitoring a building using deconvolution interferometry. II: ambient-vibration analysis. Bull Seism Soc Am 104(1):204–213

Nakata N, Snieder R, Kuroda S, Ito S, Aizawa T, Kunimi T (2013) Monitoring a building using deconvolution interferometry. I: earthquake-data analysis. Bull Seismol Soc Am 103:1662–1678

Nakata N, Tanaka W, Oda Y (2015) Damage detection of a building caused by the 2011 Tohoku-Oki earthquake with seismic interferometry. Bull Seism Soc Am 105:2411–2419

Okada S, Takai N (2000) Classifications of structural types and damage patterns of buildings for earthquake field investigation. In Proceedings of the 12th world conference on earthquake engineering, Auckland, New Zealand (Vol. 30)

Picozzi M, Parolai S, Mucciarelli M, Milkereit C, Bindi D, Ditommaso R, Vona M, Gallipoli MR, Zschau J (2011) Interferometric analysis of strong ground motion for structural health monitoring: the example of the L'Aquila, Italy, seismic sequence of 2009. Bull Seism Soc Am 101:635–651

Prieto GA, Lawrence JF, Chung AI, Kohler MD (2010) Impulse response of civil structures from ambient noise analysis. Bull Seism Soc Am 100:2322–2328

Rahmani M, Ebrahimina M, Todorovska MI (2015) Time-wave velocity analysis for early earthquake damage detection in buildings: application to a damaged full-scale RC building. Earthquake Eng Struct Dynam 44:619–636

Rossetto T, Elnashai A (2003) Derivation of vulnerability functions for European-type RC structures based on observational data. Eng Struct 25:1241–1263

Snieder R, Safak E (2006) Extracting the building response using seismic interferometry: theory and application to the Millikan Library in Pasadena. California Bull Seism Soc Am 96:586–598

Sun H, Al-Qazweeni J, Parol J, Kamal H, Chen Z, Buyukozturk O (2019) Computational modeling of a unique tower in Kuwait for structural health monitoring: numerical investigations. Struct Contr Health Monit 26:e2317

Todorovska MI, Trifunac MD (2008a) Earthquake damage detection in the Imperial County Services Building III: analysis of wave travel times via impulse response functions. Soil Dynam Earthquake Eng 28:387–404

Todorovska MI, Trifunac MD (2008b) Impulse response analysis of the Van Nuys 7-storey hotel during 11 earthquakes and earthquake damage detection. Struct Contr Health Monit 15:90–116

Vidal F, Navarro M, Aranda C, Enomoto T (2014) Changes in dynamic characteristics of Lorca RC buildings from pre-and post-earthquake ambient vibration data. Bull Earthquake Eng 12:2095–2110

Wen W, Kalkan E (2017) System identification based on deconvolution and cross correlation: an application to a 20-story instrumented building in Anchorage. Alaska Bull Seismol Soc Am 107:718–740

Zembaty Z, Kowalski M, Pospisil S (2006) Dynamic identification of a reinforced concrete frame in progressive states of damage. Eng Struct 28:668–681

Publisher's Note